Energy Storage

DOI: 10.1002/ange.200702721

3D Aperiodic Hierarchical Porous Graphitic Carbon Material for High-Rate Electrochemical Capacitive Energy Storage**

*Da-Wei Wang, Feng Li, Min Liu, Gao Qing Lu, and Hui-Ming Cheng**

Electrochemical capacitors (ECs) are essential components of high-rate electric devices used in the development of hybrid vehicles. Such capacitors are based on electrochemical charge accommodation at the electric double layer and the occurrence of Faradaic reactions.[1] Porous carbon materials, transition-metal oxides, and conducting polymers are fundamental candidates used as EC electrode materials.[1] Among the available metal oxides, RuO_2 shows the best performance, but it is very expensive.[2] Alternative cheaper oxides, such as NiO, cannot be used at voltage windows above 0.6 V; furthermore, most of them are poorly conductive.[3–4] Conducting polymers also show some drawbacks—their short cycle life being one of them.[5] As a consequence, porous carbon materials turn out to be the most promising candidates, because of their stable physicochemical properties, good conductivity, low cost, and availability.[6–8]

However, porous-carbon-based ECs are known to suffer from electrode kinetic problems that are related to inner-pore ion transport.[1,9–12] The exact mechanism of ion transport within porous textures is very complex, because the tortuosity, connectivity, size distribution, and shape of the pores, as well as the nature of the electrolyte and the solid–liquid interface, all have to be considered.[1,13–15] Among these factors, the inner-pore ion-transport resistance and the diffusion distance are the most important ones. Large values of these two parameters lead to a significant electrode-potential drop (*IR* drop) and a low ion-accessible surface area (S_{access}) at large current values, thus severely reducing the performance of the ECs.

Carbon materials with a 3D ordered/aperiodic porous texture, which facilitates ion transport by providing a smaller resistance and shorter diffusion pathways, are strongly recommended for the fabrication of advanced ECs.[15] Numerous efforts have been devoted to produce tailored porous carbon materials,[6–10,16–22] and activated or ordered mesoporous carbons have been widely studied. Microporous (> 10 μm) activated carbons (ACs) have a long diffusion distance (> 5 μm) and a high ion-transport resistance, which leads to a large *IR* drop and a small S_{access} at high current values. On the other hand, ordered mesoporous carbons (OMCs) have mesoporous channels (of about 4–6 nm) with a lower ion-transport resistance and smaller particles (exhibiting a size of 1–2 μm) with a shorter diffusion route (of 0.5–1 μm). However, the porous texture of OMCs cannot fulfill high-rate (< 2 s) ECs applications, where larger mesopores (> 10 nm) and nanometer-scale diffusion distances (< 100 nm) are required. Taking this into account, nanometer-sized OMCs could be helpful, but the aggregation of nanoparticles would become a severe problem.

Herein, we report the electrochemical performance of 3D aperiodic hierarchical porous graphitic carbon (HPGC) as a promising electrode material for high-rate EC applications. The 3D hierarchical porous texture combines macroporous cores, mesoporous walls, and micropores. The physicochemical properties of the electrolyte in the macropores are similar to those of the bulk electrolyte with the lowest resistance.[13] Ion-buffering reservoirs can be formed in the macropores to minimize the diffusion distances to the interior surfaces. Furthermore, the mesoporous walls provide low-resistant pathways for the ions through the porous particles,[10,14,19–22] and the micropores strengthen the electric-double-layer capacitance.[23–24] This 3D architecture composed of macroporous cores and mesoporous walls is self-supported and can overcome nanoparticle aggregation. In this design, three electrochemical processes are involved, namely, buffering ions in the macroporous cores, transporting ions through the mesoporous walls, and confining ions in the micropores. Moreover, the localized graphitic structure can enhance the electric conductivity. The experimental results show that both the energy and the power densities at high rate are greatly improved when HPGC replaces AC or OMC as the EC electrode material.

Liquid-nitrogen cryosorption, scanning electron microscopy (SEM), and transmission electron microscopy (TEM) studies clearly show the uniqueness of the 3D aperiodic HPGC structure. The nitrogen isotherm of the HPGC material (Figure 1 a) exhibits combined characteristics of type I/II, with a Brunauer–Emmett–Teller (BET) surface area of 970 $m^2 g^{-1}$, a total pore volume of 0.69 $cm^3 g^{-1}$, a micropore volume of 0.3 $cm^3 g^{-1}$, a micropore-to-total-pore-volume ratio of 0.43, and an average pore diameter of 2.85 nm. The pore-size distribution derived using nonlocal density functional theory (DFT) is given in Figure 1 b. Three regions can be identified: 1) ultrafine micropores (< 1 nm)

[*] D.-W. Wang, Dr. F. Li, Prof. M. Liu, Prof. H.-M. Cheng
Shenyang National Laboratory for Materials Science
Institute of Metal Research
Chinese Academy of Sciences
72 Wenhua Road, Shenyang 110016 (China)
Fax: (+86) 24-2390-3126
E-mail: cheng@imr.ac.cn
Prof. G. Q. Lu
Australian Research Council Centre for Functional Nanomaterials, AIBN and School of Engineering
The University of Queensland, QLD 4072 (Australia)

[**] The authors acknowledge financial support from the National Natural Science Foundation of China (Nos. 50472084 and 50632040).

Supporting information for this article is available on the WWW under http://www.angewandte.org or from the author.

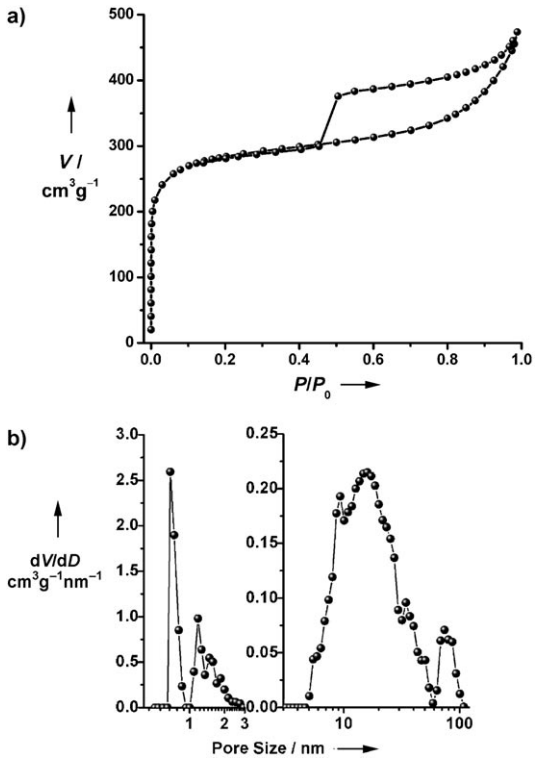

Figure 1. Nitrogen adsorption–desorption isotherm (a) and pore-size distribution (b) of the HPGC material.

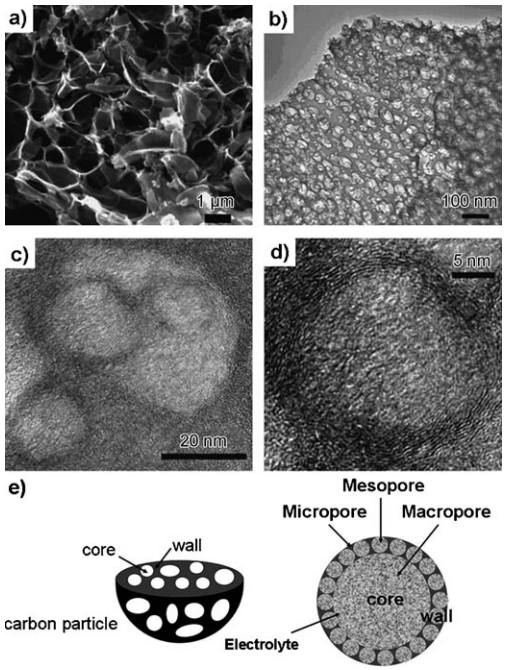

Figure 2. a) SEM image of the macroporous cores of the HPGC material, b) TEM image of the mesoporous walls, c) TEM image showing the micropores, d) high-resolution TEM (HRTEM) image of the localized graphitic mesopore walls, and e) schematic representation of the 3D hierarchical porous texture.

and micropores (1–2 nm), 2) mesopores (5–50 nm), and 3) macropores (60–100 nm). The SEM image (Figure 2a) shows the texture of the macroporous cores, which have a diameter of about 1 μm; these cores extend into the particles, thus forming ion-buffering reservoirs. The thickness of the walls around them is less than 100 nm. When the macroporous cores are immersed in the electrolyte, the thin walls around them are covered by it, thus giving a diffusion distance shorter than 50 nm. The TEM image (Figure 2b) reveals the mesoporous texture of the walls. The mesopores have diameters between 10 and 50 nm, and they can provide a short ion-transport pathway through the walls, with a minimized inner-pore resistance. There are micropores around the mesopores (Figure 2c), and the mesopore walls consist of localized graphitic structures, which leads to an enhanced electric conductivity (see Figure 2d). Extensive SEM/TEM observations (see the Supporting Information) confirm the homogeneity and characteristics of the 3D HPGC textures. The pore sizes determined from TEM measurements agree well with those derived from nitrogen adsorption analysis. A schematic illustration of a 3D hierarchical porous texture is shown in Figure 2e. The characteristics of a 3D self-supporting macroporous network, including meso–microporous walls and localized graphitic structures, make HPGC materials more convenient than hollow carbon foams or OMCs (which do not contain 3D macropores) and than ordered macroporous carbons (which do not have mesopores or graphitic structures). The new HPGC, which is unique in its structure, shows promise as a good electrode material for advanced EC technology.

The electrochemical performance of HPGC was compared to that of other porous carbon materials. In the case of HPGC, the cyclic voltammetry (CV) profiles retain a rectangular shape at all sweep rates between 20 and 200 $mV\,s^{-1}$ (Figure 3a), whereas the CV curves of CMK-3 (rod-type OMCs with *p6mm* space group) and activated carbon (AC; Maxsorb, Japan), recorded at 200 $mV\,s^{-1}$, are distorted. These results demonstrate the superior ion response of HPGC. In Figure 3b, we compare the capacitance retention ratio of HPGC with those of CMK-3, CMK-5,[19] and AC. The highest ratio (90%) was obtained in HPGC at 100 $mV\,s^{-1}$. These results highlight the suitability of HPGC for high-rate operation. Although understanding the exact mechanism of ion transport in this porous texture needs more detailed investigations, we believe that the shortened diffusion distance from the external electrolyte to the interior surfaces by ion-buffering reservoirs and the minimized ion-transport resistance in the mesoporous walls contribute synergistically to the high-rate performance. Furthermore, the localized graphitic units of HPGC lead to a lower equivalent series resistance (ESR) of 0.08 Ω relative to those of CMK-3 and AC (0.2 and 0.28 Ω, respectively) which also helps to reduce the electrode *IR* drop.

The Ragone plot of HPGC is exhibited in Figure 3c. The energy and power densities were calculated by means of constant-current charging–discharging of a supercapacitor using a cell-voltage window of 1 V and current densities between 0.02 and 50 $A\,g^{-1}$. The energy and power densities can be written, respectively, as: $E = CV^2/2$ and $P = iV/2$, where C, V, and i are the gravimetric capacitance, the cell

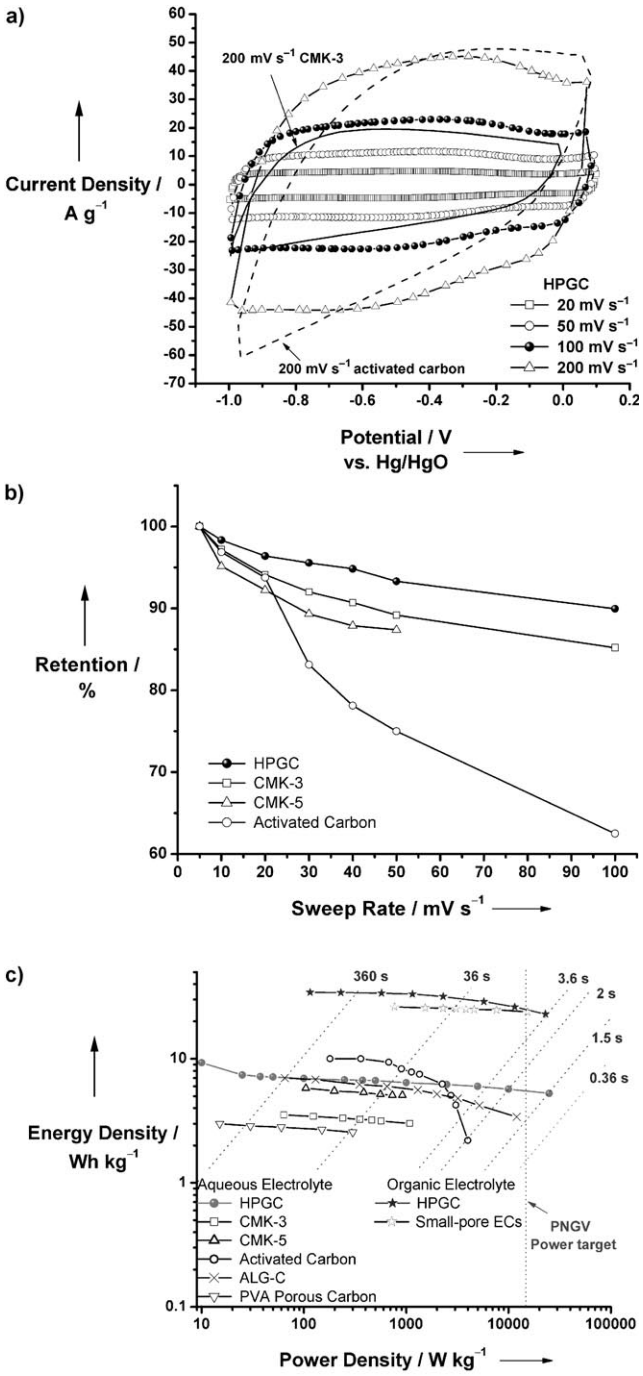

Figure 3. Electrochemical performance of the HPGC material: a) CV results measured at sweep rates of 20, 50, 100, and 200 mV s^{-1} in an alkaline electrolyte (6 mol L^{-1} KOH) within the potential range: −1.0–0.1 V (vs. Hg/HgO), b) Capacitance retention ratio as a function of the potential sweep rates, c) Ragone plot showing the position of the HPGC material relative to those of CMK-3, CMK-5,[19] activated carbon (Maxsorb, Japan), ALG-C,[16] PVA porous carbon,[22] and small-pore ECs.[23] The dotted lines show the current drain time. The weight of the cell components is not included in these *E*/*P* calculations. The *E*/*P* values used for comparison were calculated from the capacitance data given in the corresponding references. The PNGV power target (namely, 15 kW kg^{-1}, in terms of electrode active material weight) is also shown.

voltage, and the current density. At a long current drain time of 36 s, the energy and power densities of HPGC, AC, CMK-5, and ALG-C are very similar (in the range of 5–8.5 Wh kg^{-1} and 500–900 W kg^{-1}, respectively), whereas at high rates and current drain times shorter than 3.6 s, these parameters vary significantly for HPGC, AC, and ALG-C. At a time of 2 s, the values of the energy and power densities of HPGC are 5.7 Wh kg^{-1} and 10 kW kg^{-1}, respectively, whereas those of AC at the same rate are only 2.2 Wh kg^{-1} and 4 kW kg^{-1}. Moreover, at 1.5 s, $E = 5.3$ Wh kg^{-1} and $P = 25$ kW kg^{-1} for HPGC, relative to $E = 3.4$ Wh kg^{-1} and $P = 12$ kW kg^{-1} for ALG-C. More importantly, the highest power-density value measured for HPGC reached the power target of the PNGV (Partnership for a New Generation of Vehicles),[25–26] thus supporting the applicability of HPGC-based ECs as power-supply components in hybrid vehicle systems. The energy and power limitations normally observed at high rates are associated with the complexly distributed resistance and the tortuous diffusion pathways within the porous textures. At high rates, only some parts of the pores (mainly the outer regions) can be accessed by the ions, whereas at low rates, both the outer- and the inner-pore surfaces are used for charge propagation. The superior performance of HPGC at high rates clearly confirms the success of the 3D hierarchical porous texture in facilitating ion transport and keeping a higher S_{access} value for energy storage.

Very recently, Chmiola et al. discovered the anomalous electric-double-layer phenomenon in sub-nanometer pores and prepared small-pore ECs using an organic electrolyte suitable for the PNGV power target.[23] The performance of our HPGC in the same organic electrolyte was also studied for comparison (Figure 3c). Even at a current drain time of only 3.6 s, the energy and power densities of HPGC were 22.9 Wh kg^{-1} and 23 kW kg^{-1}, respectively, thereby exceeding the PNGV power target; this result is comparable to—or even better than—that obtained for small-pore ECs at a drain time of 6 s (that is, 23.8 Wh kg^{-1} and 15 kW kg^{-1}, calculated from the capacitance data given in ref. [23]). The advanced performance of the HPGC material in both organic and aqueous electrolytes confirms its universal applicability for high-rate ECs.

In summary, we demonstrate that the four characteristics of our HPGC (namely, macroporous cores as ion-buffering reservoirs, mesoporous walls with smaller ion-transport resistance, micropores for charge accommodation, and a localized graphitic structure for enhanced electric conductivity) make it a suitable electrode material for advanced ECs. The new material exhibits high energy and power densities in both aqueous and organic electrolytes. We first introduced macroporous ion-buffering reservoirs and graphitic mesopore walls with excellent electric conductivity into the EC electrode materials to produce an HPGC structure that is capable of overcoming the primary kinetic limits of electrochemical processes in porous electrodes. Considering the wide applications of porous carbon materials in electrochemistry, we think that this concept can be extended for enhancing the performance of different electrochemical systems.

Experimental Section

Although non-silica oxides, such as MgO[22] and TiO_2,[27] have been used to prepare porous carbons, we used the alkaline system $Ni(OH)_2$/NiO to prepare the porous carbon materials. Our strategy was to start by adding a solution of phenolic resin in ethanol into the alkaline $Ni(OH)_2$ solution to obtain a homogeneous hydroxide/resin system. Upon slow evaporation of the solvent in a glass utensil, a composite of inorganic and resin materials was obtained, from which the HPGC was separated after carbonization and template removal. Details of the synthesis are provided in the Supporting Information.

The material was characterized by means of nitrogen cryosorption (Micromeritics, ASAP 2010M), SEM (LEO, SUPRA 35, 15 kV), and TEM (JEOL JEM-2010, 200 kV). Details of the electrochemical characterization are given in the Supporting Information.

Received: June 21, 2007
Revised: August 12, 2007
Published online: November 19, 2007

Keywords: electrochemical capacitors · electrochemistry · energy storage · ion channels · mesoporous materials

[1] B. E. Conway, *Electrochemical Supercapacitors: Scientific Fundamentals and Technological Applications*, Kluwer Academic/Plenum Publishers, New York **1999**.
[2] J. P. Zheng, T. R. Jow, *J. Electrochem. Soc.* **1995**, *142*, L6.
[3] W. Xing, F. Li, Z. F. Yan, G. Q. Lu, *J. Power Sources* **2004**, *134*, 324.
[4] S. H. Lee, C. E. Tracy, J. R. Pitts, *Electrochem. Solid-State Lett.* **2004**, *10*, A229.
[5] V. Khomenko, E. Frackowiak, F. Béguin, *Electrochim. Acta* **2005**, *50*, 2499.
[6] R. Kötz, M. Carlen, *Electrochim. Acta* **2000**, *45*, 2483.
[7] E. Frackowiak, F. Béguin, *Carbon* **2001**, *39*, 937.
[8] A. G. Pandolfo, A. F. Hollenkamp, *J. Power Sources* **2006**, *157*, 11.
[9] D. Qu, H. Shi, *J. Power Sources* **1998**, *74*, 99.
[10] D. W. Wang, F. Li, H. T. Fang, M. Liu, G. Q. Lu, H. M. Cheng, *J. Phys. Chem. B* **2006**, *110*, 8570.
[11] H. K. Song, Y. H. Jung, K. H. Lee, L. H. Dao, *Electrochim. Acta* **1999**, *44*, 3513.
[12] H. K. Song, H. Y. Hwang, K. H. Lee, L. H. Dao, *Electrochim. Acta* **2000**, *45*, 2241.
[13] D. R. Rolison, *Science* **2003**, *299*, 1698.
[14] G. Lee, S. Pyun, *Langmuir* **2006**, *22*, 10659.
[15] J. W. Long, B. Dunn, D. R. Rolison, H. S. White, *Chem. Rev.* **2004**, *104*, 4463.
[16] E. Raymundo-Piñero, F. Leroux, F. Béguin, *Adv. Mater.* **2006**, *18*, 1877.
[17] D. Hulicova, J. Yamashita, Y. Soneda, H. Hatori, M. Kodama, *Chem. Mater.* **2005**, *17*, 1241.
[18] D. Hulicova, M. Kodama, H. Hatori, *Chem. Mater.* **2006**, *18*, 2318.
[19] W. Xing, S. Z. Qiao, R. G. Ding, F. Li, G. Q. Lu, Z. F. Yan, H. M. Cheng, *Carbon* **2006**, *44*, 216.
[20] A. B. Fuertes, F. Pico, J. M. Rojo, *J. Power Sources* **2004**, *133*, 329.
[21] H. Yamada, H. Nakamura, F. Nakahara, I. Moriguchi, T. Kudo, *J. Phys. Chem. C* **2007**, *111*, 227.
[22] T. Morishita, Y. Soneda, T. Tsumura, M. Inagaki, *Carbon* **2006**, *44*, 2360.
[23] J. Chmiola, G. Yushin, Y. Gogotsi, C. Portet, P. Simon, P. L. Taberna, *Science* **2006**, *313*, 1760.
[24] E. Raymundo-Piñero, K. Kierzek, J. Machnikowski, F. Béguin, *Carbon* **2006**, *44*, 2498.
[25] B. Scrosati, *Nature* **1995**, *373*, 557.
[26] R. F. Nelson, *J. Power Sources* **2000**, *91*, 2.
[27] C. A. Filho, A. J. Zarbin, *Carbon* **2006**, *44*, 2869.

